American Mineralogist, Volume 65, pages 1087–1102, 1980

Contact-metamorphic effects of the Stillwater Complex, Montana: the concordant iron formation

D. T. VANIMAN, J. J. PAPIKE AND T. LABOTKA

Department of Earth and Space Sciences
State University of New York
Stony Brook, New York 11794

Abstract

Archaean iron formation (>3.1 b.y.), contact-concordant at the base of the Stillwater Igneous Complex, Montana, was contact-metamorphosed to temperatures >800°C at a pressure ≥2 kbar. Temperature estimates are based on the presence of low-Ca, Fe-rich pyroxene with two-stage exsolution textures suggesting inversion from Fe-pigeonite; the thermal stability of identical pyroxene compositions is known from experimental data. The assemblage fayalite–magnetite–quartz is rarely found; rather, the fO_2-dependent assemblage orthopyroxene–magnetite–quartz is common throughout the iron formation. Comparisons with the younger (~2 b.y.) contact-metamorphosed Gunflint Iron Formation, Minnesota, show striking similarities in composition and conditions of metamorphism: both iron formations were metamorphosed at fO_2 conditions near fayalite–magnetite–quartz stability. In contrast, the available data for regionally-metamorphosed iron formations show that they reach comparable temperatures at higher fO_2. The distinctive low fO_2 of contact-metamorphosed iron formations reflects restriction of fO_2 under the influence of the contacting igneous body. Exchange along fractures in the Stillwater Iron Formation included limited introduction of Cu, S, and Al, probably from the Stillwater Complex.

Introduction

The Stillwater Igneous Complex of southwestern Montana is a large layered mafic intrusion dipping to the north and exposed for about 50 km along an east–west strike. The basal contact of the igneous complex is well exposed, although no roof contacts have been found. Page and Nokleberg (1974) made a detailed 1:12,000 map of the basal igneous complex and underlying hornfels, and Page (1977) described the petrography of the igneous and contact-metamorphic rocks. Their studies show a common sequence of metapelite–iron formation–blue quartzite–metapelite along traverses from the base of the igneous complex into the contact-concordant hornfels. The metamorphic grade near the contact is within the pyroxene–hornfels facies; the assemblage cordierite + hypersthene + ilmenite + plagioclase + biotite + quartz occurs in pelitic rocks. Most exposures of iron formation have thinly interbedded metapelites of the pyroxene–hornfels facies, although metapelites below the iron formation in the Boulder River Valley are of the hornblende–hornfels facies (orthopyroxene absent). Our major purpose is to evaluate the metamorphic conditions within the iron formation at five localities along the base of the igneous intrusion. Petrologic study of these samples shows a common peak intensity of thermal metamorphism throughout the iron formation, and reveals restricted chemical exchange during metamorphism.

Comparisons with the Gunflint Iron Formation, Minnesota

In many respects, the contact metamorphism of the Gunflint Iron Formation by the Duluth Igneous Complex in Minnesota is similar to the metamorphism of the iron formation below the Stillwater Igneous Complex. Simmons *et al.* (1974) estimate a pressure of metamorphism (≥2 kbar) and thermal regime (≥800°C) similar to minimum P,T conditions we suggest for the iron formation below the Stillwater Igneous Complex. Bulk analyses of the metamorphosed Gunflint Iron Formation are not available for comparison, but the unmetamorphosed Biwabik Iron Formation, which is correlative with the metamor-

0003–004X/80/1112–1087$02.00

phosed Gunflint Iron Formation, is compositionally similar to the Stillwater Iron Formation. The greatest differences between the unmetamorphosed Biwabik and the metamorphosed Stillwater Iron Formation (Table 1) are the Fe^{2+}/Fe^{3+} ratios and CO_2 contents; when metamorphic effects are negated by using total atomic Fe for comparison and normalizing the Biwabik to a CO_2-free analysis, the similarities between the two iron formations are striking. Both the Stillwater and Gunflint Iron Formations have been metamorphosed by contact with large (>2500 km^3) mafic intrusions. Comparisons with the Gunflint Iron Formation throughout this report are based on these similarities.

Despite major similarities, certain differences between the Gunflint and Stillwater occurrences are critical: (1) The Stillwater Iron Formation is contact-concordant; in no case has it been found directly in contact with the basal Stillwater norite. Where exposed, there is a minimum of 3 m of pelitic hornfels between the iron formation and the basal Stillwater igneous rocks. This relationship is not found in the Duluth Complex (Fig. 1), where the iron formation can be traced into the igneous contact. (2) The Stillwater Iron Formation is more than a billion years older than the Gunflint Iron Formation (Nunes and Tilton, 1971, and Page, 1977, estimate an age for the Stillwater Iron Formation between 3.1 and 3.7 b.y.; Hanson and Malhotra, 1971, estimate that the Gunflint Iron Formation is ~2 b.y. old). The comparability in major-element composition (Table 1) suggests similar origins, for both are 'Lake Superior Type' banded iron formations (Eichler, 1976). However, despite the comparable banded textures in both localities, the Gunflint Iron Formation can be traced into unmetamorphosed iron formation away from the contact whereas the unmetamorphosed equivalent of the Stillwater Iron Formation has not been found. Therefore the prograde destruction of ooid textures and carbonate assemblages documented in Minnesota (Floran and Papike, 1975) is not seen in Montana. Ooid structures and Fe-bearing carbonates were probably part of the premetamorphic Stillwater Iron Formation, but these features can only be proposed and not proven. (3) Simmons *et al.* (1974) suggest that the Gunflint Iron Formation has been modified by introduction of Al and Ti from the Duluth Complex, where the Gunflint rocks are enriched in plagioclase and ilmenite adjacent to the contact. This type of enrichment occurs but is not as prominent in the Stillwater Iron Formation.

Table 1. Bulk composition of iron formations

	unmetamorphosed Biwabik Iron Formation(*)	metamorphosed Stillwater Iron Formation(**)
SiO_2	46.40	45.31
Al_2O_3	0.90	1.79
TiO_2	0.04	0.04
Fe_2O_3	18.70	14.49
FeO	19.71	28.42
MnO	0.63	0.11
MgO	2.98	3.73
CaO	1.60	1.14
Na_2O	0.04	0.01
K_2O	0.13	0.08
CO_2	6.90	0.03
Fe/(Fe+Mg)	0.84	0.90

(*)from Eichler (1976); wet-chemical analysis.
(**)average of five rapid-rock analyses by H. Smith reported in Page (1977).

The study of Simmons *et al.* (1974) on high-grade Gunflint Iron Formation near the Duluth Igneous Complex was based on a single sample. Floran and Papike (1978) studied the broader field relations of the contact-metamorphic effects on the Gunflint Iron Formation and recognized four metamorphic zones based on the first appearances of key iron-rich index minerals (greenalite, minnesotaite, grunerite, and ferrohypersthene). The greenalite zone represents essentially unmetamorphosed rocks, and metamorphic effects (the appearance of minnesotaite and magnetite) occur more than 5 km from the contact. Ferrohypersthene appears as far as 1 km from the contact. Such detailed mapping based on key index minerals is not possible in the associated pelitic rocks; Labotka *et al.* (in preparation) find that discontinuous metamorphic reactions within pelitic rocks occur only within a few tens of meters from the contact with the Duluth Complex. This is not the case at the basal Stillwater contact zone, where Page and Nokleberg (1974) mapped biotite–, hornblende–, and pyroxene–hornfels zones, with biotite hornfels grading into the older regional-metamorphic terrane of the Beartooth Mountains about 10 km from the igneous contact. Because the Stillwater Iron Formation occurs paral-

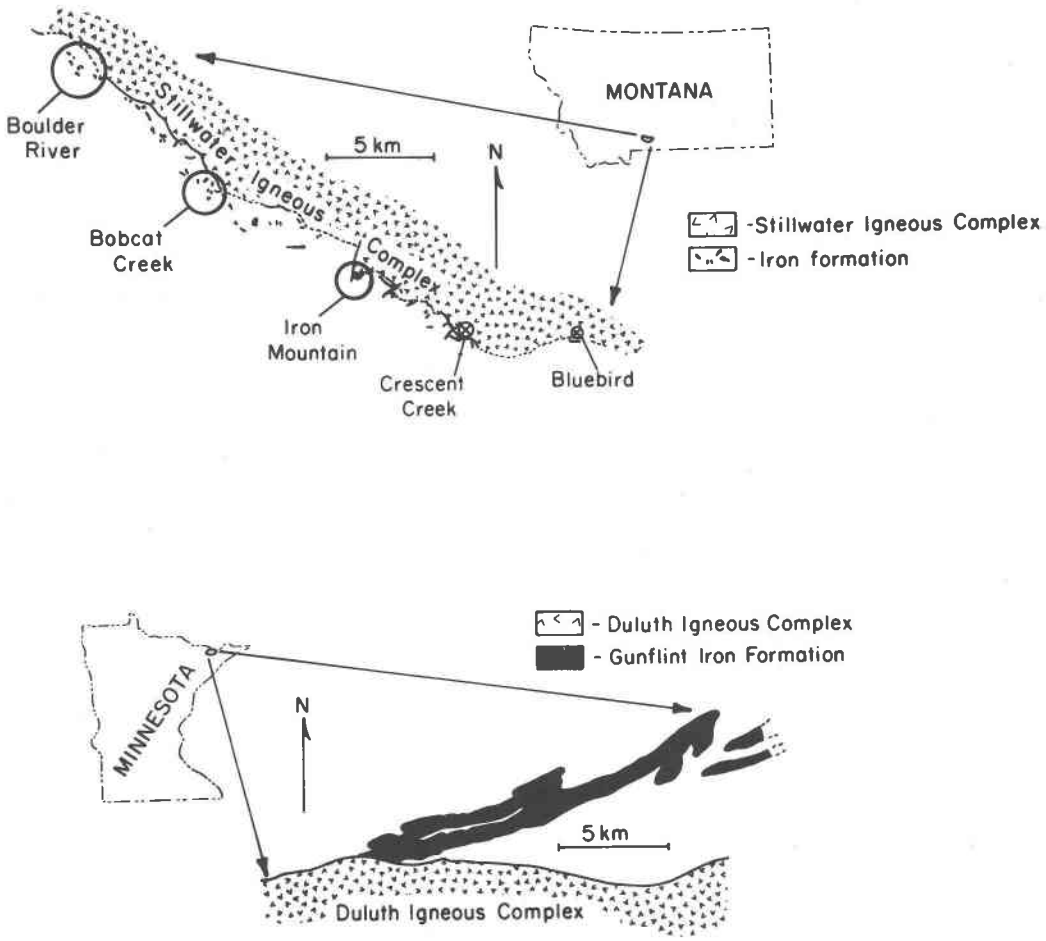

Fig. 1. Relative distribution of concordant iron formation below the Stillwater Complex, and discordant Gunflint Iron Formation intersecting the Duluth Complex. Note that the faulted, discontinuous but concordant iron formation below the Stillwater Complex dips steeply to the north; the relatively undisturbed Gunflint Iron Formation dips shallowly (<20°) to the south.

lel to and within meters of an igneous contact (it is entirely equivalent with the ferrohypersthene zone of Floran and Papike, 1978), a prograde zonation of key index minerals is not observed. Instead, since the Stillwater Iron Formation was raised concordantly to a uniform peak of thermal metamorphism, it is appropriate to examine the petrographic variations due to minor differences in original bulk composition or to exchange with the adjacent pluton.

Methods

Field studies were conducted during the summers of 1976 and 1978. These studies were keyed to sampling traverses through pelitic and iron-formation sequences (Fig. 1). For a map base the authors relied heavily on the published map of Page and Nokleberg (1974).

Mineral analyses were obtained on an ARL-EMX SM automated microprobe with one semi-fixed spectrometer (for Si) and three positionable spectrometers. Data were reduced by the matrix correction procedures of Bence and Albee (1968) and Albee and Ray (1970). The determinations of Fe^{2+}/Fe^{3+} in amphiboles and oxides were made by the recalculation technique of Papike *et al.* (1974). All microprobe data were collected with a focused beam (~2 μm), except in traverses across exsolved hedenbergite, ferroaugite, or ferropigeonite with a 20 μm broad-beam to estimate the original compositions prior to exsolution.

Petrology of pelitic rocks associated with the iron formation

The Stillwater Iron Formation is locally interbedded with pelitic rocks. Table 2 lists the common mineral assemblages in pelitic rocks adjacent to iron

Table 2. Pelitic assemblages

	Orthopyroxene	Cummingtonite	Tremolite	Biotite	Cordierite	Plagioclase	Almandine	Ilmenite	Chromite	Fe Sulfide	Fe-Ni Sulfide	Fe-Cu Sulfide	Quartz
Boulder River													
29B	X(0.42)				X(0.38)	X(An83)		X					
27B			X(0.25)	X(0.40)		X(An55)		X					X
26D	X(0.55)			X(0.53)	X(0.38)			X	X				X
Bobcat Creek													
13XB	X(0.58)			X(0.57)	X(0.38)	X(An36)		X		X	X	X	X
13J	X(0.58)			X(0.57)	X(0.39)	X(An30)		X		X			
16E		X(0.52)		X(0.51)		X		X		X		X	X
Iron Mountain													
18	X(0.48)			X(0.47)	X(0.30)			X		X			
Crescent Creek													
426	X(0.50)	X(0.49)			X(0.31)			X		X	X		X
432.5	X(0.52)			X(0.65)	X(0.32)	X(An47)		X		X			X
433	X(0.51)				X(0.32)		X(0.87)	X	X				X
436	X(0.50)				X(0.31)	X		X	X	X			
Bluebird													
none													

Numbers in parentheses are Fe/(Fe + Mg), or An/(An + Ab) in plagioclase.

formation below the Stillwater Complex. The five localities indicated in Table 2 (Boulder River, Bobcat Creek, Iron Mountain, Crescent Creek, and Bluebird) are shown in Figure 1. The three westernmost localities are exposed at the surface, but the two easternmost localities (Crescent Creek and Bluebird) are drill-core samples, with sample numbers that indicate footage along the drill string (Tables 2 and 4a,b). Both drill cores were collected by drilling through a sequence of the basal Stillwater Complex and into the underlying contact zone (Fig. 1). These core samples were generously provided by Norman Page of the U.S. Geological Survey and by the Anaconda Company of Butte, Montana.

Pelitic assemblages intercalated with iron formation were all formed within the pyroxene–hornfels facies. The characteristic assemblage of this facies in the Stillwater metapelitics is orthopyroxene–cordierite–ilmenite (Table 2). Pyroxenes within the pelitic pyroxene–hornfels assemblages have a common range of compositions at all localities [Fe/(Fe + Mg) ratio (Fe′) = 0.42–0.58, av. 0.51], but cordierites are consistently more Mg-rich (Fe′ = 0.31) in the eastern localities (Crescent Creek, Bluebird, and Iron Mountain) than at the western localities (Fe′ = 0.38). Other phases include biotite, chromite, and Fe–Cu–Ni sulfides. Almandine occurs in only one sample (433) within the Crescent Creek drill core. These assemblages are summarized in Al–Fe–Mg diagrams (Fig. 2), and representative analyses are listed in Table 3.

Petrology of the iron formation

Iron formation samples represent each of the five localities for which pelitic assemblages have been described (Table 2, Fig. 1). The iron formation assemblages have been divided into olivine-free (Table 4a), quartz-free (Table 4b), and fayalite–magnetite–

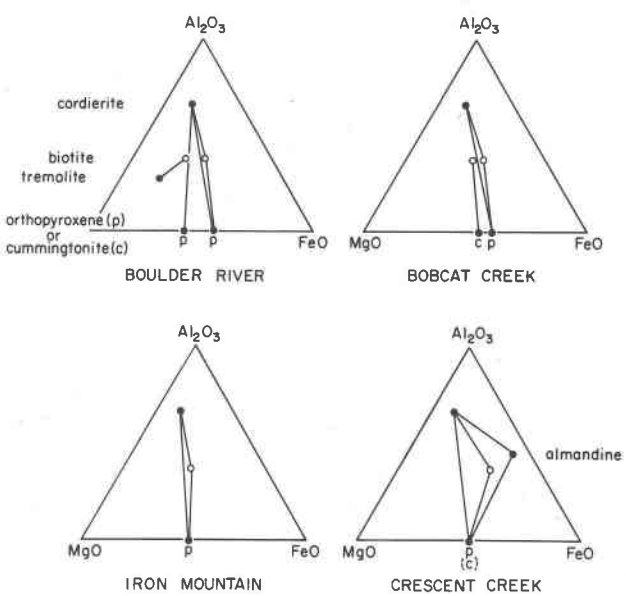

Fig. 2. Pelitic assemblages occuring with iron formation below the Stillwater Complex. Overlapping tie-lines can be resolved by referring to Table 2 for other phases involved in the projection. Dashed parentheses (Crescent Creek) indicate coexisting orthopyroxene plus cummingtonite.

Table 3. Mineral compositions: pelitic rocks

	Sample 26D Biotite	Sample 16E Cummingtonite	Sample 29B Orthopyroxene	Sample 13XB Cordierite	Sample 432.5 Plagioclase	Sample 433 Almandine	Sample 13XB Ilmenite
SiO_2	35.5	50.1	52.1	48.6	57.6	37.4	
Al_2O_3	17.3	3.62	0.48	32.9	27.4	22.1	0.28
TiO_2	3.3	0.31	0.18	0.0	0.0	0.0	53.2
FeO	19.3	26.9	26.8	8.7	0.30	36.5	46.8
Fe_2O_3*		0.2					
MnO	0.02	0.36	0.41	0.06	0.0	1.29	0.71
MgO	9.5	13.9	19.1	8.0	0.0	2.96	0.0
CaO	0.0	0.27	0.88	0.04	9.4	1.75	0.0
Na_2O	0.12	0.04	0.0	0.11	6.0	0.0	0.0
K_2O	8.7	0.02	0.0	0.01	0.04	0.0	0.0
Cr_2O_3	0.79	0.14	0.04	0.0	0.0	0.0	0.0
(H_2O)	5.5	4.1		1.6			
Σ	100.0	100.0	100.0	100.0	100.7	102.0	101.0
Si	5.45	7.62	1.98	5.00	2.56	2.95	
Al^{IV}	2.55	0.38	0.02	1.00	1.44	0.05	0.01
Al^{VI}	0.57	0.27		2.99		2.01	0.99
Ti	0.38	0.04	0.01	0.0	0.0	0.0	0.97
Fe^{2+}	2.48	3.41	0.85	0.75	0.01	2.41	0.02
Fe^{3+}*		0.02					
Mn	0.0	0.05	0.01	0.0	0.0	0.08	0.0
Mg	2.17	3.14	1.08	1.23	0.0	0.35	0.0
Ca	0.0	0.04	0.04	0.0	0.45	0.15	0.0
Na	0.04	0.01	0.0	0.02	0.52	0.0	0.0
K	1.69	0.0	0.0	0.0	0.0	0.0	0.0
Cr	0.10	0.02	0.0	0.0	0.0	0.0	0.0
$\Sigma_{cations}$	15.43	15.00	3.99	10.99	4.98	8.00	1.99
Fe/(Fe+Mg)	0.53	0.52	0.44	0.38	1.0	0.87	1.0

*Fe_2O_3 calculated for amphibole only (Papike et al., 1974)
(H_2O) estimated for biotite, amphibole and cordierite
Analyses normalized to (n) oxygens: biotite (22), amphibole (23), pyroxene (6), cordierite (18), plagioclase (8), almandine (12), ilmenite (3).

quartz (Table 4c) assemblages. The olivine-free assemblages all contain magnetite + quartz ± one or two pyroxenes and low-Ca amphibole, with a notable absence of minor phases except chlorine-rich biotite. Quartz-free assemblages contain either high-Ca clinopyroxene or orthopyroxene, + olivine and magnetite, with a much greater variety of minor phases (plagioclase, K-feldspar, apatite, ilmenite, pyrite, pyrrhotite, chalcopyrite) than are found in the olivine-free assemblages. The fayalite–magnetite–quartz assemblage at Boulder River includes hedenbergite. A distinction is made between specific 'orthopyroxene' in quartz-free assemblages and general 'low-Ca pyroxene' in olivine-free assemblages, for exsolution textures and reconstructed pyroxene compositions indicate that some of the 'low-Ca pyroxenes' in Table 4a are inverted pigeonites. Representative mineral compositions from the iron formation are listed in Table 5, and reconstructed estimates of pigeonite, augite, and hedenbergite (prior to exsolution) are listed in Table 6.

Only the prograde iron formation assemblages are listed in Tables 4a,b,c, and only those amphiboles which appear to be primary (large subhedral grains with equilibrated boundaries against adjacent minerals) are included. It is not always possible to identify retrograde *vs.* prograde amphiboles, though retrograde textures are often evident where amphibole forms a pseudomorph after another phase (*e.g.*, fayalite). Those amphiboles which have been characterized as 'retrograde' have Fe′ ratios ranging from 0.65 to 0.91 at all localities except in the drill cores (Crescent Creek and Bluebird), where retrograde amphibole may have Fe′ values of 0.48 to 0.63. 'Primary' amphiboles at all localities (Table 4a) are cummingtonite–grunerite grains with an Fe′ range of 0.58 to 0.89. Thus there is no obvious compositional distinction between prograde and retrograde amphi-

Table 4a. Iron formation assemblages (olivine-free)

	Low-Ca Pyroxene	High-Ca Pyroxene	Quartz	Magnetite	Cummingtonite-Grunerite	Other
Boulder River						
Z3B	X(0.76)*	X(0.70)	X	X		
Z4		X(0.63)	X	X	X(0.70)	
Z5		X(0.80)	X	X	X(0.85)	
26G			X	X	X(0.67)	
34A	X(0.75)		X	X	X(0.76)	biotite(0.77)
43A		X(0.65)	X	X	X(0.60-0.74)	
Bobcat Creek						
13XC	X(0.80)		X	X	X(0.79)	biotite(0.85)
Iron Mountain						
19D	X(0.72)		X	X		
19F		X(0.62)	X	X		
Crescent Creek						
none						
Bluebird						
171-176	X(0.72)*		X	X		
184-190	X(0.68)		X	X		
222-228			X	X	X(0.69-0.73)	biotite(0.92)

Numbers in parentheses are Fe/(Fe+Mg) atomic.
* Host composition of inverted pigeonite.

Table 4b. Iron formation assemblages (quartz-free)

	Orthopyroxene	High-Ca Clinopyroxene	Olivine	Magnetite	Other
Boulder River					
Z6	X(0.64)		X(0.85)	X	
26F		X(0.81-0.89)	X(0.97)	X	
28	X(0.68)		X(0.85)	X	plagioclase, An84
34B	X(0.70-0.75)		X(0.89)	X	
Bobcat Creek					
9F		X(0.73)	X(0.97)	X	
9G		X(0.71)	X(0.97)	X	apatite
9H		X(0.76-0.89)	X(0.96)	X	K-feldspar
Iron Mountain					
none					
Crescent Creek					
44B			X(0.84)	X	
Bluebird					
176-177	X(0.66)		X(0.81)	X	
177-181			X(0.83)	X*	
190-195	X(0.64)			X	ilmenite, pyrrhotite
200	X(0.61)		X(0.82)	X	
210			X(0.80)	X*	
218-221	X(0.53)			X	
231-235	X(0.65)		X(0.86)	X	
251-254	X(0.75)		X(0.96)		ilmenite, pyrite, chalcopyrite

Numbers in parenthesis are Fe/(Fe+Mg) atomic.
* Magnetite with hercynite + ilmenite exsolution.

boles in the western occurrences, but retrograde amphiboles in the drill cores may be distinctly Mg-rich. The possibility of some exchange with fluids from the Stillwater Complex during retrograde amphibole growth is discussed in a later section. All amphiboles in the iron formation are poor in 'others' components (Al, Ti, Cr, Fe^{3+}, Mn, K, Na), and all but a few are very low in Ca. Analyses of 'retrograde' (448) as well as 'prograde' (9E) amphiboles are listed in Table 5.

Grain sizes in the iron formation are generally less than 1 mm but range up to 3 mm in single equant crystals of quartz, olivine, or orthopyroxene and may exceed 2 cm in poikiloblastic crystals of orthopyroxene inverted from ferropigeonite. The common size range for all silicates, however, is 0.1–1.0 mm. Magnetite occurs most commonly in the same size range as the associated Fe,Mg-silicates (except where it is associated with larger poikiloblastic inverted pigeonites). Magnetite may be as large as 3–5 mm where associated with large equant 3 mm olivine.

Mineral grains are generally equant and anhedral to subhedral throughout the iron formation. Exceptions occur where euhedral secondary amphiboles have formed, often grown across the equilibrated contacts between equant primary phases. There are common textural styles, dependent on mineral type, which characterize the prograde minerals (Fig. 3).

Poikiloblastic: ferropigeonites inverted to orthopyroxene
equant anhedral: orthopyroxene, augite, hedenbergite, olivine, magnetite
irregular anhedral: quartz
subequant subhedral: amphibole

Retrograde minerals occur as polycrystalline pseudomorphs after prograde minerals (*e.g.*, $Mg_{0.5}Fe_{0.5}$ amphibole replacing $Mg_{0.15}Fe_{0.85}$ olivine, Fig. 4a,b), as penetrative growth across equilibrated grain contacts (*e.g.*, orthopyroxene replacing olivine), or as a replacement of primary phases along fractures.

Cm-scale structures within the iron formation are finely banded, but banding seldom extends for more than a few cm without chaotic disruption. Cm-sized blocks with mm-scale banding occur as brittle clasts surrounded by quartz flowage and quartz–magnetite recrystallization. In less chaotic areas where cm-scale banding is preserved, the banding may often pinch and swell and microboudins of ferromagnesian sili-

Table 4c. Iron formation assemblage with fayalite–magnetite–quartz

	High-Ca Clinopyroxene	Olivine	Quartz	Magnetite
Boulder River 35A	X(0.71)	X(0.93)	X	X

Table 5. Mineral compositions: iron formation

	Sample 9E	Sample 448	Sample 3B		Sample 19F		Sample 26F	Sample 28	Sample 9F	Sample 9B	Sample BB210
	Cummingtonite	Cummingtonite	Host orthopyroxene	Lamella augite	Lamella Low-Ca pyroxene	Host augite	Host hedenbergite	olivine	olivine	magnetite	hercynite (lamella in magnetite)
SiO_2	50.4	53.8	48.4	50.3	48.2	50.7	48.4	31.3	30.6	0.51	0.00
Al_2O_3	0.48	0.22	0.93	1.40	0.30	0.23	1.93	0.30	0.45	0.34	61.0
TiO_2	0.04	0.0	0.02	0.0	0.04	0.05	0.13	0.04	0.05	0.05	0.12
FeO	36.9	27.9	39.9	22.7	42.2	20.3	25.4	62.6	67.4	31.4	35.6
Fe_2O_3*	0.1	0.3								66.5	
MnO	0.56	0.17	0.20	0.04	0.19	0.04	0.02	0.24	1.06	0.0	0.09
MgO	8.1	15.8	8.9	6.6	8.1	7.0	3.50	6.2	1.55	0.0	3.75
CaO	0.67	0.33	1.48	20.7	0.87	21.2	21.2	0.02	0.08	0.07	0.0
Na_2O	0.0	0.0	0.0	0.0	0.0	0.0	0.0	0.0	0.0	0.0	0.0
K_2O	0.03	0.0	0.0	0.0	0.0	0.0	0.0	0.0	0.0	0.0	0.0
Cr_2O_3	0.02	0.05	0.03	0.0	0.04	0.02	0.0	0.0	0.0	0.0	0.05
(H_2O)	2.7	1.4									
Σ	100.0	100.0	99.9	101.7	99.9	99.5	100.6	100.7	101.2	98.9	100.6
Si	7.94	7.95	1.98	1.96	1.99	2.00	1.94	1.00	1.00	0.02	0.0
Al^{IV}	0.06	0.04	0.02	0.04	0.01		0.06			0.02	2.00
Al^{VI}	0.03		0.02	0.02		0.01	0.03	0.01	0.02		
Ti	0.0	0.0	0.0	0.0	0.0	0.0	0.0	0.0	0.0	0.0	0.0
Fe^{2+}	4.86	3.44	1.36	0.74	1.46	0.67	0.85	1.68	1.85	1.02	0.83
Fe^{3+}*	0.01	0.03								1.94	
Mn	0.07	0.02	0.01	0.0	0.01	0.0	0.0	0.01	0.03	0.0	0.0
Mg	1.90	3.47	0.54	0.38	0.49	0.41	0.21	0.30	0.08	0.0	0.16
Ca	0.11	0.05	0.06	0.86	0.04	0.89	0.91	0.0	0.0	0.0	0.0
Na	0.0	0.0	0.0	0.0	0.0	0.0	0.0	0.0	0.0	0.0	0.0
K	0.01	0.0	0.0	0.0	0.0	0.0	0.0	0.0	0.0	0.0	0.0
Cr	0.0	0.01	0.0	0.0	0.0	0.0	0.0	0.0	0.0	0.0	0.0
$\Sigma_{cations}$	14.99	15.01	3.99	4.00	4.00	3.98	4.00	3.00	2.98	3.00	2.99
Fe/(Fe+Mg)	0.72	0.50	0.72	0.66	0.75	0.62	0.80	0.85	0.96	1.0	0.84

*Fe^{3+} estimated for amphibole and magnetite
Analyses normalized to (n) oxygens: amphiboles (23), pyroxenes (6), olivines (4), magnetite and hercynite (4).

cates plus magnetite occur within the more ductile quartz-rich bands. These features suggest considerable deformation during metamorphism. The irregular passage from coherent banding to chaotic structure in single hand samples may indicate internal disruption as well as deformation in response to external stresses; this internal disruption may occur as a result of a 10–20% volume loss such as Floran and Papike (1978) have attributed to decarbonation in contact metamorphism of the Gunflint Iron Formation.

Mineralogy of the iron formation

Orthopyroxene and inverted pigeonite

Compositions of pyroxene host crystals and exsolved lamellae are listed in Table 5. In Table 6, pigeonite compositions have been reconstructed from multiple broad-beam (~20 μm) microprobe analyses of orthopyroxene host and augite lamellae. All pyroxenes approach pure stoichiometric Ca,Mg,Fe compositions with insignificant amounts of minor elements (M sites contain less than 2% ^{VI}Al or Mn, tetrahedral sites have less than 2% ^{IV}Al). These relatively pure 'quadrilateral' compositions allow direct comparison of the pyroxene data to experimental results on the pure Ca–Mg–Fe system.

The presence of prograde pigeonite is inferred from the occurrence of two sets of Ca-pyroxene exsolution lamellae within some poikiloblastic orthopyroxenes; one set is thick (≤0.05 mm), blebby, and randomly oriented, and the other set is thin (<0.001 mm), straight, and oriented parallel to (100) of the host orthopyroxene (Fig. 5b). Bonnichsen (1969), in describing pyroxenes from the metamorphosed Biwabik Iron Formation of Minnesota, attributed this two-stage exsolution texture to exsolution both prior to and following the inversion of pigeonite to orthopyroxene. Bonnichsen pointed out that the 'randomly' oriented sets of thick lamellae were in fact exsolved on an older set of (001) planes in small grains of pigeonite. These smaller pigeonite grains coalesced into a single large orthopyroxene upon inversion from monoclinic ($P2_1/c$) to orthorhombic (*Pbca*) structure. The growth of several pigeonites into a single larger orthopyroxene is favored by the sluggish nucleation rate of orthopyroxene; it is easier for a pigeonite to recrystallize with the orientation of a neighboring pigeonite already inverted to *Pbca* than it is for the $P2_1/c$ grain to invert on its own. The

Table 6. Reconstructed* pyroxene compositions (prior to exsolution)

	(Coexisting in Sample 23B)		Sample 26F
	Pigeonite	Augite	Hedenbergite
SiO_2	47.80	49.90	48.80
Al_2O_3	0.90	1.70	1.27
TiO_2	0.0	0.0	0.15
FeO	40.40	26.40	29.30
MnO	0.17	0.04	0.12
MgO	7.40	6.50	1.94
CaO	3.45	16.00	19.60
Cr_2O_3	0.0	0.0	0.06
Σ	100.10	100.50	101.20
Si	1.96	1.97	1.97
Al^{IV}	0.04	0.03	0.03
Al^{VI}	0.0	0.05	0.03
Ti	0.0	0.0	0.0
Fe	1.39	0.87	0.99
Mn	0.01	0.0	0.0
Mg	0.45	0.38	0.12
Ca	0.15	0.68	0.85
Cr	0.0	0.0	0.0
Σcations	4.00	3.98	3.99
Wo	7.7	35.1	43.4
En	22.7	19.9	5.9
Fs	69.6	45.1	50.7

*reconstructions made from sets of 10 to 20 broad-beam (20 μm) analyses made in traverses across single crystals.

difficulty of nucleating orthopyroxene is commonly encountered in experimental studies on Fe-rich systems (D. H. Lindsley, personal communication), and this difficulty may account for the extended poikiloblastic growth of orthopyroxenes (many are >1 cm) from smaller precursor pigeonites (~1 mm) in the Stillwater Iron Formation. Similar features are described by Simmons *et al.* (1974) from the Gunflint Iron Formation near the contact with the Duluth Complex.

The presence of inverted-pigeonite textures is evidence for metamorphism to temperatures above the lower thermal stability of ferropigeonite. The Fe/(Fe + Mg) ratio (Fe′) we have calculated for the high-temperature ferropigeonite (Table 6) in the Stillwater Iron Formation is 0.75. This Fe′ composition is identical to that used by Simmons *et al.* and by Podpora and Lindsley (1979) for experiments on the *P,T* conditions of orthopyroxene–ferropigeonite transition. Simmons *et al.* determined that the three-phase field (augite + pigeonite + orthopyroxene) is stable at 800°C and 2 kbar. Podpora and Lindsley, starting with augite and orthopyroxene, produced pigeonite + orthopyroxene + augite at 825°C. These experiments suggest that the three-pyroxene stability field is at 800–825°C for 2 kbar and Fe′ = 0.75. Simmons *et al.* also pointed out that 2 kbar is a minimum pressure for the production of ferropigeonite in their experiments, because at lower pressures the ferropigeonite would have disproportionated to form a more Mg-rich pigeonite + fayalite + quartz.

The acceptance of 800–825°C as a minimum temperature depends on the assumption that pigeonite did not nucleate and grow below its field of minimum thermal stability. The textures of inverted pigeonites described above are evidence of the relative ease of pigeonite nucleation (many individual grains), in contrast with the sluggish nature of orthopyroxene nucleation (a few poikiloblastic grains). Pigeonite may nucleate below its field of thermal stability if it formed from a non-pyroxene assemblage of low thermal stability, rapidly brought to high temperature. This metastable nucleation of pigeonite was observed in the synthesis runs of Simmons *et al.* in which they generated starting materials, and it may also occur during contact metamorphism of an iron formation which is rapidly brought from low-temperature conditions to pyroxene–hornfels conditions. Thus some form of independent evidence is needed to show that pigeonite was in its stability field if the 800–825°C minimum temperature is to be applied to naturally-occurring metamorphosed iron formations. Pigeonite stability is indicated in the Stillwater Iron Formation by the rather large grain size (~1 mm) of precursor pigeonite domains in the poikiloblastic orthopyroxenes, and by evidence of subequant (*i.e.*, equilibrated) grain shapes in reconstructions of the outlines of pre-inversion pigeonites (Fig. 5b). This evidence for intergrowth with surface equilibrium between grains is an indication of long-term annealing at high temperature with attainment of intercrystalline equilibrium. For this reason we propose ferropigeonite stability and a minimum metamorphic temperature of 800–825°C for those samples of the Stillwater Iron Formation with inverted-pigeonite textures.

Samples with inverted-pigeonite texture are found at the Boulder River and Bluebird localities (Fig. 1). These localities are the westernmost and easternmost limits of our sampling range, and suggest that the estimated peak of metamorphic temperature (800–825°C) was attained along the entire length of the contact-concordant iron formation. The absence of inverted-pigeonite textures at intermediate localities

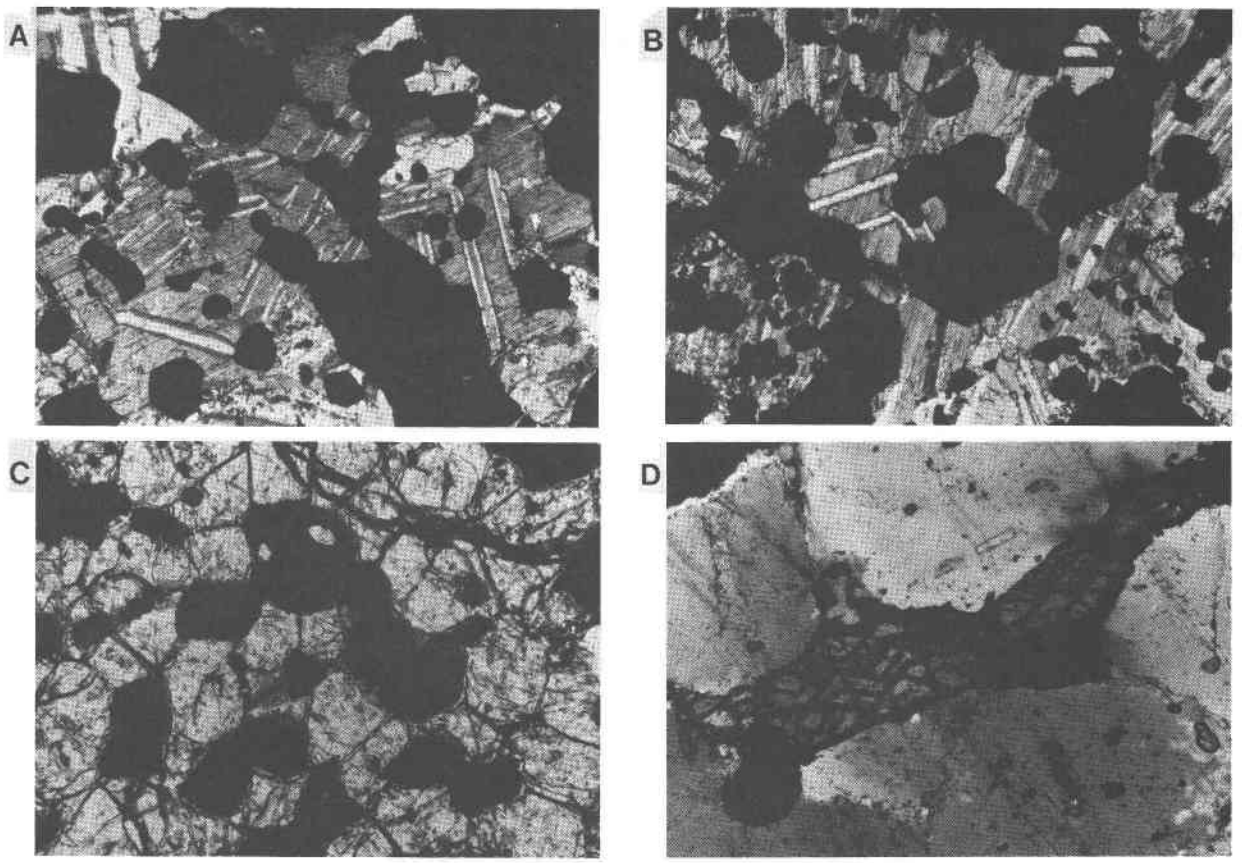

Fig. 3. Prograde mineral textures, Stillwater iron formation. The poikiloblastic orthopyroxenes in sample 171-176 (A,B) inverted from numerous smaller pigeonite grains, each with its own set of thick relic (001) lamellae that mark the various orientations of pre-inversion pigeonites. Note included magnetite, and continuous thin (100) lamellae trending NE to NNE in these photographs. Olivine and magnetite grains in sample 177–181 (C) are anhedral and equant, with polygonal grain boundaries. (D) shows subequant, subhedral amphibole in a matrix of coarse irregular, anhedral optically-strained quartz, sample 43A. Bottom dimension of each photograph is 1.75 mm.

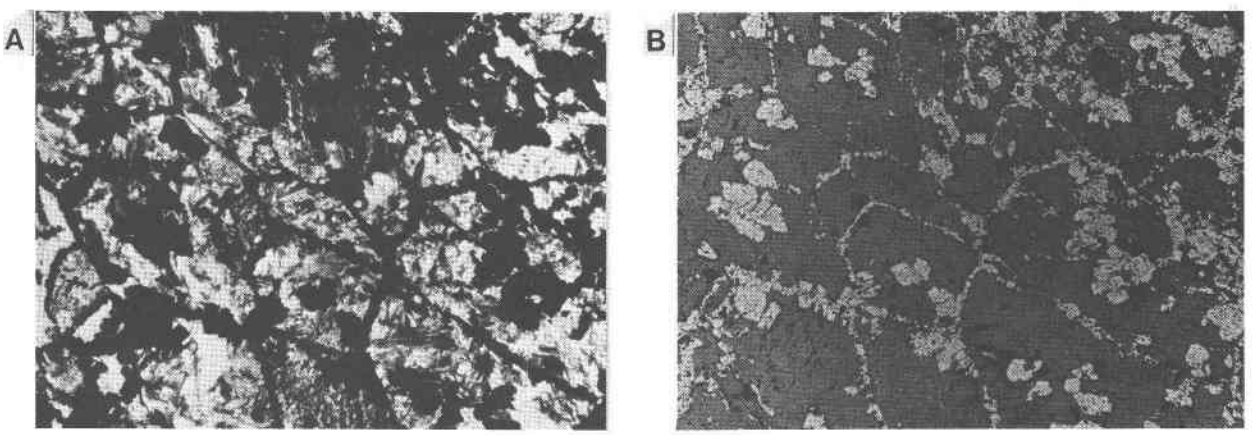

Fig. 4. Fibrous retrograde cummingtonite forming pseudomorphs after olivine with magnetite rims in sample 9A. Photograph (A) is in transmitted light with crossed polars; photograph (B) taken in reflected light. Bottom dimension of each photograph is 1.75 mm.

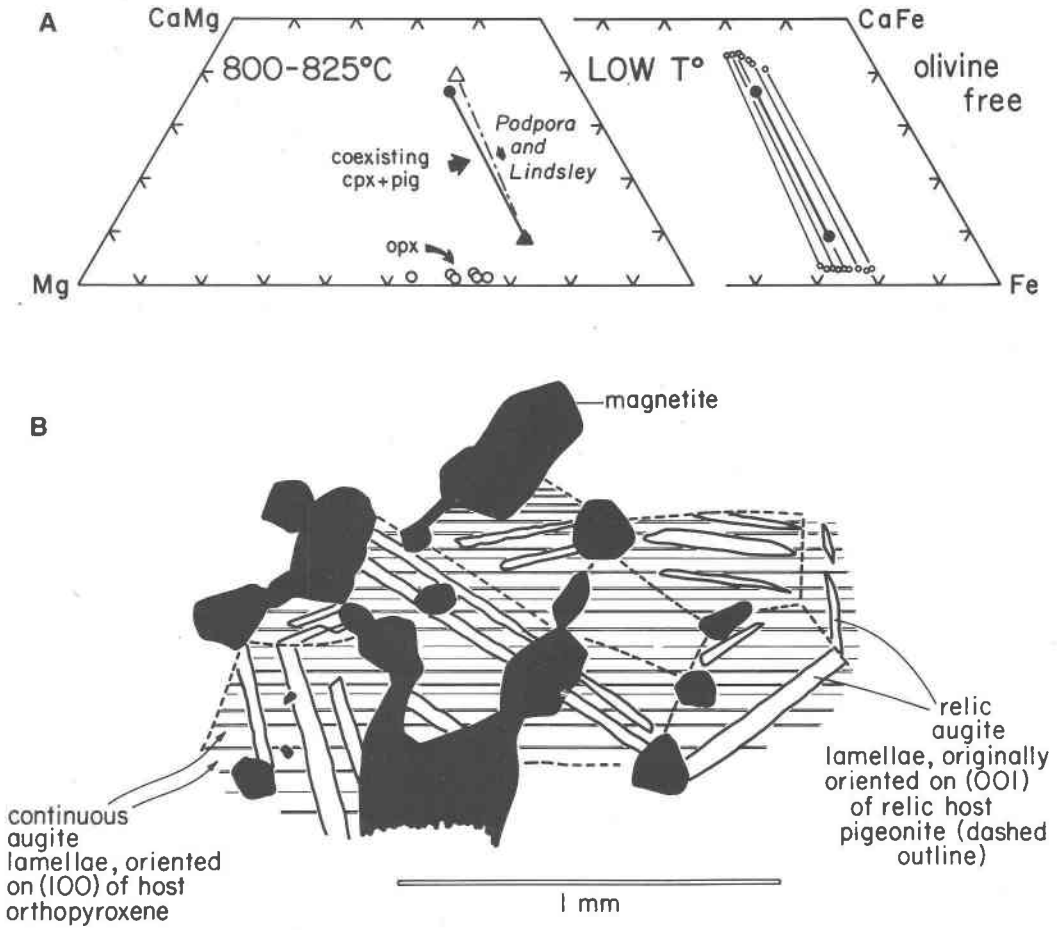

Fig. 5. (A) Ca–Mg–Fe compositions of inverted pigeonite and coexisting augite prior to exsolution (solid symbols) and following exsolution (small open symbols). The reconstructed pigeonite–augite compositions are also shown on the 800–825°C diagram, along with the experimental data of Podpora and Lindsley (1979) for coexisting pigeonite–augite at this temperature range (triangles), and the compositions of Stillwater Iron Formation orthopyroxenes (open circles) that are too Ca-poor to form pigeonite at this temperature. (Note that orthopyroxenes also occur in the range Fe′ = 0.70–0.80, but these are considered to represent re-equilibration at lower temperature.)

(B) Single poikiloblastic orthopyroxene (sample 171–176) including at least seven equant anhedral pigeonites; the limits of each precursor pigeonite (dashed lines) are marked by the extent of their relic (001) lamellae (thick bars). The crystallographic continuity of the poikiloblastic orthopyroxene is indicated by continuity of later (100) lamellae, exsolved at lower temperature from the *Pbca* structure.

is a reflection of variation in bulk composition rather than variation in temperature of metamorphism; orthopyroxenes without inverted-pigeonite texture occur in rocks with very Ca-poor bulk compositions, or in rocks with a higher Fe/(Fe + Mg) composition that favors the formation of hedenbergite plus olivine rather than augite plus pigeonite (Table 4).

Augite and hedenbergite

Of the five localities sampled below the Stillwater Igneous Complex (Fig. 1), only the three western localities contain iron formation with Ca content high enough to form augite or hedenbergite during prograde metamorphism. The decrease of Ca contents to the east, coupled with a decrease in overall Si content (a decrease in the abundance of quartz banding), is the most apparent lateral variation within the Stillwater Iron Formation. In the western localities, augite ($Wo_{35}En_{20}Fs_{45}$) occurs in contact with inverted pigeonites. The augites have (001) exsolution lamellae of pigeonite (clinopyroxene $P2_1/c$ structure 'locked in' by the host $C2/c$ structure) despite entry into the *Pbca* orthopyroxene stability field on cooling. Host and lamellae compositions of exsolved aug-

ite are listed in Table 5. In extremely Ca- and Fe-rich rocks at the Boulder River and Bobcat Creek localities, hedenbergite with extremely fine lamellae of ferropigeonite occurs. The pre-exsolution bulk compositions of hedenbergite hosts plus lamellae were obtained by broad-beam microprobe analysis (Table 6). Compositions of host hedenbergite can be obtained directly by focused-beam microprobe analysis (Table 5). Lamellae of ferropigeonite in hedenbergite can be characterized by their cell parameters (Table 7) even though the pigeonite lamellae are too fine for microprobe analysis. Attempts to estimate the ferropigeonite compositions from cell parameters (*e.g.,* the b–β nomograms of Papike *et al.,* 1971; Brown, 1960; Matsui *et al.,* 1968) for both our data and those of Simmons *et al.* (1974) point to anomalously small b dimensions in the exsolved ferropigeonite. The values of β suffer less from distortion and provide reliable estimates of Ca content. From the β angle of exsolved ferropigeonite in sample 26F, and the range of Fe′ estimated from the trends of combined host–lamellae microprobe data, we obtain an estimated composition of $Wo_{5-6}En_{11-17}$ for the exsolved pigeonite in Table 7.

Olivine

Olivine occurs in the Stillwater Iron Formation in equilibrium with magnetite and either quartz, orthopyroxene, or Fe-rich clinopyroxene. In the Ca-poor eastern portion of the iron formation (Crescent Creek and Bluebird), there are cm-scale layers composed entirely of olivine (Fa 84) plus magnetite, or olivine (Fa 96) plus ilmenite. However, the association of Fa 81–85 olivine with orthopyroxene is common throughout the iron formation, and an association of Fa 93–98 olivine with augite/hedenbergite is common in Ca-rich bands of the western iron formation (Table 4b). At only one locality near Boulder River are olivine and quartz found in contact. However, in many samples olivine may be separated from quartz by orthopyroxene-rich bands of less than 1 cm. Simmons *et al.* (1974) found that quartz and olivine were not in contact in the Gunflint Iron Formation but were separated by as little as 20 μm of orthopyroxene. From this they concluded that the activity of SiO_2 was only slightly less than unity; from the use of Williams' (1972) data for coexisting Fe-rich olivine and pyroxene they calculated a SiO_2 activity of 0.9 to 0.95. The generally greater separation (>1 cm) between olivine and quartz in the Stillwater Iron Formation suggests a lower activity of SiO_2 in most samples, though a SiO_2 activity of essentially 1.0 is evident in sample 35A from the Boulder River where fayalite + magnetite + quartz occur intergrown.

Table 7. Cell parameters of hedenbergite host and pigeonite lamellae; precession camera data (sample 26F)

	a(Å)	b(Å)	c(Å)	α	β	γ	V(Å^3)
hedenbergite host	9.85	9.00	5.25	90°	105°13′	90°	449
pigeonite lamellae	9.75	9.00	5.24	90°	108°35′	90°	436

Fe(Ti,Al) oxides

Magnetite is the common oxide in all the iron formation assemblages, with the sole exception of the orthopyroxene (Fe′ = 0.75)–fayalite (Fa 96)–ilmenite sample BB 251-254 in the Bluebird drill core (in the absence of magnetite, the orthopyroxene–fayalite assemblage in this sample is comparatively Fe-rich). In general, all magnetite is stoichiometric Fe_3O_4 with only trace amounts of Al (~0.3%) and no other minor constituents in significant concentration. Exsolution occurs in small lamellae near the limits of optical resolution or is not visible at all, with the exception of samples from the 182- to 215-foot depth interval in the Bluebird drill core, where magnetite may contain 5% hercynite as oriented lamellae (Table 5) and $\ll$1% ilmenite as irregular exsolved pods. Although the magnetite compositional deviations in this part of the Bluebird drill core are exceptional, the compositions of the coexisting silicates (*e.g.,* olivine, orthopyroxene) do not differ significantly in major- or minor-element composition from olivine–orthopyroxene–pure Fe_3O_4 assemblages elsewhere in the iron formation (BB 231-235, Boulder River 28 and 26). One sample (BB 190-195) is bracketed by layers of the Bluebird core which have magnetite with visible hercynite and ilmenite exsolution, yet the sample BB 190-195 has pure Fe_3O_4 coexisting with a few discrete grains of ilmenite: both oxides are stoichiometrically pure, and have evidently re-equilibrated at low temperature.

Primary and secondary (retrograde) amphiboles

Amphibole grains, which are large (>0.2 mm), subhedral, and confined to bands of quartz–magnetite ± high-Ca pyroxene, appear to have equilibrated with other prograde minerals and are therefore interpreted as primary. Retrograde amphiboles form pseudomorphs after a primary mineral (*e.g.,* olivine, see Fig. 4a and 4b) or grow across equilibrated grain boundaries between primary minerals. Figure 6 com-

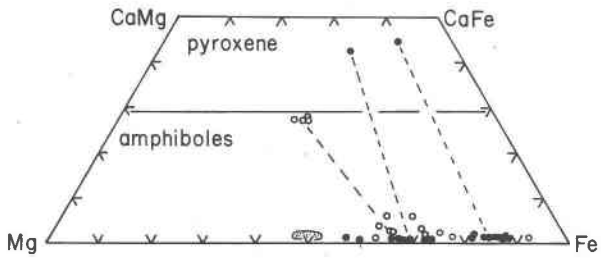

Fig. 6. Amphiboles (and coexisting clinopyroxene) in the Stillwater Iron Formation. Solid symbols represent prograde amphibole compositions; open symbols represent retrograde amphibole compositions (pseudomorphs after other minerals, or other texturally secondary amphiboles). Note that retrograde amphiboles tend to be more Ca-rich, and include actinolites. The stippled area at Fe′ ~ 0.5 shows the field of Mg-rich retrograde fracture-filling amphiboles found in the Bluebird drill core.

pares the compositions of these 'primary' and 'secondary' amphiboles. Most amphiboles are Ca-poor, with the exception of a few occurrences of secondary tremolite replacing hedenbergite. The primary amphiboles form two main groups, Fe-cummingtonite with Fe′ = 0.65 to 0.73, and grunerite with Fe′ = 0.82 to 0.89 (Fig. 6). Primary Fe-cummingtonite and grunerite may occur at a single locality (*e.g.*, Boulder Creek; Table 4a), but not within the same hand sample. The bimodality in primary amphibole compositions apparently represents a bimodality in original bulk compositions.

Amphiboles with Fe′ 0.62 to 0.80 occur throughout the iron formation as replacements of original orthopyroxene (with little or no Fe–Mg exchange) or as replacements of olivine, with substantial Mg enrichment in the replacement process. In most of the iron formation, the secondary growth of Mg-enriched amphibole after Fe-rich olivine may be accomplished by oxidation of olivine to form magnetite plus amphibole, *e.g.*:

$$2H_2O + 3O_2 + 16Fe_{1.7}Mg_{0.3}SiO_4 \rightarrow 2Fe_{4.6}Mg_{2.4}Si_8O_{22}(OH)_2 + 6Fe_3O_4$$

Evidence for this reaction is found where stringers of magnetite are intergrown with amphibole in the replacement of olivine. A special group of Mg-rich secondary amphiboles occur as replacements of olivine or along small sulfide-filled fractures in the drill cores of the eastern iron formation (Bluebird and Crescent Creek localities). These especially Mg-rich cummingtonites (Fe′ = 0.48 to 0.53) are found only in the eastern part of the iron formation and do not contain any second-generation magnetite associated with amphibole growth.

Biotite

Prograde biotite is rare, occurring only at the Boulder River locality and in the Bluebird drill core with grunerite (Fe′ = 0.76–0.83), magnetite, and quartz ± orthopyroxene (Fe′ = 0.75). The biotite is Fe-rich annite (Fe′ = 0.77–0.92), extremely poor in minor elements, with only K as an interlayer cation. Qualitative energy-dispersive microprobe analysis reveals a considerable amount of Cl in the formula.

Sulfides

Olivine-bearing assemblages in the Bluebird drill core contain pyrite (FeS_2), pyrrhotite ($Fe_{1-x}S$), and chalcopyrite ($CuFeS_2$). These sulfides occur as minor grains within the groundmass, as fracture fillings, and as large poikiloblastic grains (>1 cm) in extremely fractured portions of the drill core. The association with fractures suggests that Cu and S were introduced along fractures during late-stage alteration of the iron formation.

Conditions of metamorphism

The two-stage exsolution patterns of augite exsolved within low-Ca pyroxene indicate a metamorphic temperature in excess of 800°C. Further evidence of high temperature is found in the partition of Mg and Fe between pyroxene and olivine throughout the iron formation. Williams (1972) has pointed out that this Fe/Mg partitioning is in general a poor geothermometer because of its lack of thermal sensitivity in the pyroxene–olivine system. However, Smith (1971) described the temperature and pressure dependence of olivine and pyroxene compositions as constrained by the "forbidden region" that limits the stability of Fe-rich compositional variation in coexisting orthopyroxene + olivine + quartz at 1 kbar over a range of temperatures, and at 900°C over a range of pressures. His data require only slight extrapolation to determine phase compositions at 2 kbar and 800–825°C. The Fe/(Fe+Mg) ratio in orthopyroxene + olivine at 800–825°C corresponds well with our independent estimate of 800–825°C for the minimum temperature at the peak of metamorphism in samples within a few meters of the basal Stillwater igneous contact.

The reconstructed phase relations for the anhydrous ferromagnesian silicates are shown in Figure 7. The solid tie-lines drawn in Figure 7 are those which pertained at the peak of metamorphism; dashed tie-lines suggest assemblages which could be stable but have not been observed. Note that the

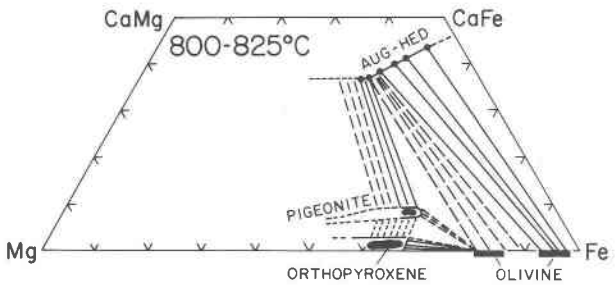

Fig. 7. Synthesis of pyroxene data inferred to occur at 800–825°C, ≥2kbar in the Stillwater Iron Formation. Solid tie-lines represent observed assemblages; dashed tie-lines represent assemblages inferred but not observed. Note that tie-lines between hedenbergite tend toward anomalously restricted olivine compositions (minimum fayalite content = 0.93), suggesting that the tie-lines in this region may connect with olivine that has re-equilibrated to higher Fe contents at lower temperatures. Orthopyroxenes also occur in the range Fe′ = 0.72–0.80 but are not considered in the construction of this diagram; these Fe-rich orthopyroxenes commonly coexist with Fe-rich olivine (fayalite 0.89–0.96) and apparently indicate local re-equilibration around the 'forbidden region' at lower temperature (extrapolation of the data of Smith, 1971, suggests a re-equilibration temperature of about 600–650°C).

solid tie-lines between hedenbergite–augite and fayalite *in orthopyroxene-free assemblages* consistently trend toward a restricted range of Fe-rich olivine composition (Fa 93–97); the tie-lines in this region may reflect olivine compositions which have re-equilibrated with magnetite at lower temperature (olivine + magnetite + quartz → more Fe-rich olivine). Orthopyroxene compositions from Fe′ = 0.72 to 0.80 are not plotted in Figure 7; these Fe-rich orthopyroxenes commonly coexist with Fe-rich olivine (samples 34B and 251–254 in Table 4b), which suggests re-equilibration across the "forbidden region" at lower temperatures (extrapolation from the data of Smith, 1971, suggests re-equilibration to ~650°C).

The Fe′ separation between coexisting olivine and orthopyroxene, shown in Figure 7, is constant throughout the Stillwater iron formation. The $K_D = (X^{Fe}_{opx}/X^{Fe}_{ol}) \cdot (X^{Mg}_{ol}/X^{Mg}_{opx})$ is ~0.32 in the metamorphosed Stillwater Iron Formation; a very similar K_D (~0.31) can be calculated for the high-grade (≥800°C) Gunflint Iron Formation studied by Simmons *et al.* (1974). However, the theoretical and experimental data of Williams (1972) extrapolate to a much higher K_D (~0.5) for this compositional range. Smith (1971) noted this discrepancy when he conducted experiments on Fe-rich olivine–orthopyroxene systems (bulk rock Fe′ > 0.7), and suggested that the data for Mg-rich olivine–orthopyroxene pairs cannot be extrapolated to high-Fe compositions. The natural and calculated K_D's are compared in Figure 8.

At a minimum temperature ≥800°C and estimated pressure of ~2 kbar, the metamorphism of the Stillwater Iron Formation is very similar to the conditions described by Simmons *et al.* for the highest grade of metamorphism of the Gunflint Iron Formation. With similar pressure, temperature, and bulk composition, it is of interest to compare the indicators of fO_2 for both localities. Figure 8 shows that although the olivine–orthopyroxene $K_D^{Fe,Mg}$ is similar for both localities, the Fe,Mg-silicates are more Fe-rich in the Gunflint Iron Formation: fayalite and orthopyroxene in the Gunflint Iron Formation were able to take more Fe into solid solution than fayalite and orthopyroxene in the Stillwater Iron Formation, without oxidizing to form magnetite and quartz. Simmons *et al.* suggested that the fO_2 during metamorphism of the Gunflint Iron Formation was slightly less than FMQ (fayalite–magnetite–quartz) stability at ≥800°C (Fig. 9). The relatively oxidized compositions of fayalite + magnetite + quartz and fayalite + orthopyroxene in the Stillwater Iron Formation indicate a slightly higher fO_2 during metamorphism, between the values for FMQ and Ni–NiO (Nitsan, 1974; Fisher, 1966).

Contact-metamorphosed iron formations, as exemplified by the Stillwater and Gunflint occurrences, were formed under relatively low fO_2 conditions recorded by the presence of olivine and magnetite. Regionally-metamorphosed iron formations, however, tend to form under conditions of higher fO_2 (Klein, 1966, 1973, 1978; Butler, 1969; Jaffe *et al.*, 1978; Immega and Klein, 1976), where olivine is not stable and hematite as well as magnetite may occur at the peak of metamorphism (Fig. 9). Not only does the presence of olivine indicate a lower fO_2 in contact-metamorphosed iron formations, but the oxide assemblages are simpler in the contact-metamorphosed than in the regionally-metamorphosed iron formations. Klein (1973) pointed out that regionally-metamorphosed iron formations tend to have banded oxide–oxide and oxide–silicate buffer systems (hematite–silicate, hematite–magnetite, magnetite–silicate) that reflect the behavior of O_2 as an initial value component with a chemical potential buffered by the local assemblage. This does not seem to be the case for the contact-metamorphosed iron formations (*e.g.*, the Stillwater and Gunflint Iron Formations), which have single-oxide (magnetite) assemblages (lacking hematite) throughout, with close proximity of faya-

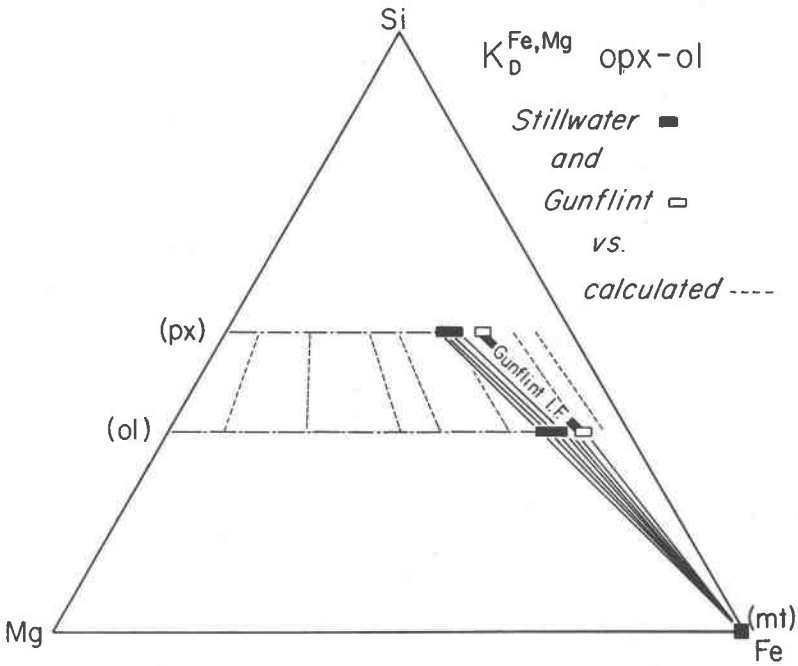

Fig. 8. Distribution of Fe,Mg between coexisting orthopyroxene and olivine. Dashed tie-lines represent the experimental data of Williams (1972) for Mg-rich compositions, with extrapolation to more Fe-rich compositions. Extrapolation to Fe-rich compositions does not fit the observed orthopyroxene–olivine compositions observed in the Gunflint and Stillwater Iron Formations, because the Fe-content of orthopyroxene is fixed at low values by the region structurally 'forbidden' to Fe-rich pyroxene.

litic olivine and quartz, which suggests fO_2 near (though not necessarily fixed at) that required for the stability of fayalite + magnetite + quartz. Both the low fO_2 and the loss of banded internal oxide buffers suggest that fO_2 is controlled by the igneous body. Figure 9 shows that theoretically and empirically determined fO_2 values for mafic igneous bodies fall along a cooling path close to but on the fO_2-poor side of the Stillwater/Gunflint Iron Formation T-fO_2 regime. Haggerty (1976) pointed out the consistency of this T-fO_2 path in the cooling histories of layered igneous intrusions. We propose that the low fO_2 and the loss of internally buffered fO_2 variability in contact-metamorphosed iron formations is due to redox interaction with the adjacent intrusions.

Relations to the Stillwater Complex

Bulk-sample analyses of pelitic rocks lead to conflicting views about chemical exchange with the Stillwater Complex. Beltrame and Larsen (1974) suggested addition of Fe, Mg, Co, Cr, Cu, Ni, and Zn from the Stillwater Complex, whereas Barker (1975) proposed that K and Rb have been depleted from pelitic rocks as far as 3000 feet from the contact. Our petrologic and microprobe data show small amounts of chromite, Fe–Cu sulfide, and Fe–Ni sulfide in pelitic rocks of both the pyroxene–hornfels and hornblende–hornfels facies. Present textural relations suggest that the chromite and sulfides were in equilibrium with the cordierite–ilmenite–Fe,Mg silicate assemblages during metamorphism. Cr, Ni, and Cu may have been introduced from the Stillwater Complex into these pelitic rocks, but large-scale mass transfer of major elements is unsubstantiated.

Iron-formation samples provide evidence of limited chemical interaction with the Stillwater Complex. Samples from the Boulder River, Crescent Creek, and Bluebird localities contain Fe–Cu sulfides and feldspars which may be due to Cu and Al addition, possibly through fluids from the Stillwater Complex. Sulfides in particular are concentrated in fractures that pass through the iron formation samples. Simmons *et al.* (1974) also suggested that the presence of feldspar in the Gunflint Iron Formation was due to near-contact introduction of Al from the igneous body.

Perhaps the best evidence for introduction of chemical components from the Stillwater Complex is in the formation of secondary cummingtonite (Fe′ = 0.50) in concentrations along sulfide-filled fractures.

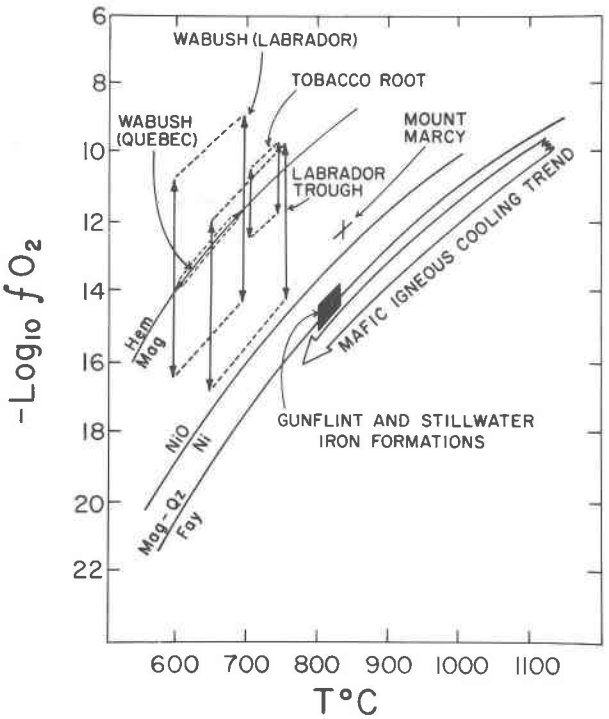

Fig. 9. Diagram of T-fO_2 conditions for contact metamorphism of the Gunflint and Stillwater Iron Formations, contrasted with regional metamorphism of comparable iron formations. The T-fO_2 trend for cooling mafic magmas follows a characteristic path (Haggerty, 1976) shown below the curve of fayalite–magnetite–quartz equilibrium; thus the T-fO_2 conditions in the Gunflint and Stillwater Iron Formations are at or slightly higher than the assumed T-fO_2 path of their contacting mafic intrusions. In marked contrast are the higher fO_2 conditions of iron formations regionally metamorphosed at comparable or lower temperatures. Data for Wabush (Quebec) are from Butler, 1969; data for Wabush (Labrador) are from Klein, 1966; data for Tobacco Root are from Immega and Klein, 1976; data for Labrador Trough are from Klein, 1978. Data for Mount Marcy are from Jaffe *et al.*, 1978, based on oxide data alone.

In some samples (*e.g.*, Bluebird 200) the area within a few mm of the fracture has been replaced entirely by this relatively magnesian amphibole (Fe′ = 0.50), whereas the remainder of the rock contains an iron-formation assemblage with Fe′ > 0.75. The formation of the Mg-rich amphiboles from the relatively Fe-rich rock may be related to the formation of the sulfide veins through a reaction such as:

Fe-rich amphibole + S_2 =
Mg-rich amphibole + Fe-sulfide

Conclusions

The Stillwater Iron Formation provides mineralogical constraints on minimum prograde temperature near the contact (≥800°C). The oxygen fugacity during metamorphism was similar to that of the assemblages described by Simmons *et al.* (1974) for the highest grade in the Gunflint contact zone near the Duluth Complex: both the Stillwater and Gunflint contact rocks were near FMQ at ~800°C (fO_2 ~ 10^{-14} to 10^{-15} atm). This fO_2 value is lower than the common fO_2 values of regionally-metamorphosed iron formations, and may reflect the influence of the adjacent igneous intrusion on redox conditions in the iron formations. The Stillwater Iron Formation was open to late prograde or retrograde chemical exchange along fractures, with introduction of S (and/or Mg?) in the alteration of Fe-silicates, of Cu in the formation of Fe,Cu-sulfides, and of Al in the formation of secondary feldspar. The most likely source for these constituents is the Stillwater intrusion.

Acknowledgments

Special thanks are extended to James E. Adler and G. G. Brox of the Anaconda Company, Butte, Montana, who gave us permission to study drill core samples from the Crescent Creek and Bluebird localities. Norman Page's (U.S. Geological Survey, Menlo Park, California) help in sample selection of core materials from the Crescent Creek locality is very much appreciated. Thanks go to Ms. Robin Spencer who typed the manuscript and to Pauline Papike for technical help in putting the manuscript together. We are grateful to Bob Coleman and Norman Page for constructive reviews of the manuscript.

This research was funded by NSF grant EAR 7723150, which we gratefully acknowledge.

References

Albee, A. L. and L. Ray (1970) Correction factors for electron probe microanalysis of silicates, oxides, carbonates, phosphates, and sulfates. *Anal. Chem., 42,* 1408–1414.

Barker, R. W. (1975) Metamorphic mass transfer and sulfide genesis, Stillwater Intrusion, Montana. *Econ. Geol., 70,* 275–298.

Beltrame, R. and L. H. Larsen (1974) Probable Fe–Mg metasomatism in metasediments at the base of the Stillwater Complex, Montana (abstr.). *Geol. Soc. Am. Abstracts with Programs, 6,* 425.

Bence, A. E. and A. L. Albee (1968) Empirical correction factors for electron microanalysis of silicates and oxides. *J. Geol., 76,* 382–403.

Bonnichsen, B. (1969) Metamorphic pyroxenes and amphiboles in the Biwabik Iron Formation, Dunka River area, Minnesota. *Mineral. Soc. Am. Spec. Pap., 2,* 217–241.

Brown, G. M. (1960) The effect of ion substitution on the unit cell dimensions of the common clinopyroxenes. *Am. Mineral., 45,* 15–38.

Butler, P., Jr. (1969) Mineral compositions and equilibria in the metamorphosed iron formation of the Gagnon region, Quebec, Canada. *J. Petrol., 10,* 56–101.

Eichler, J. (1976) Origin of the Precambrian banded iron formations. In K. H. Wolf, Ed., *Handbook of Strata-bound and Stratiform Ore Deposits, 7,* 157–201. Elsevier, New York.

Fisher, G. W. (1966) Fe–Mg olivine solid solutions. *Carnegie Inst. Wash. Year Book, 65,* 209–217.

Floran, R. J. and J. J. Papike (1975) Petrology of the low grade rocks of the Gunflint Iron-Formation, Ontario–Minnesota. *Geol. Soc. Am. Bull., 86,* 1169–1190.

——— and ——— (1978) Mineralogy and petrology of the Gunflint Iron Formation, Minnesota–Ontario: correlation of compositional and assemblage variations at low to moderate grade. *J. Petrol., 19,* 215–288.

Haggerty, S. E. (1976) Opaque mineral oxides in terrestrial igneous rocks. In D. Rumble III, Ed., *Oxide Minerals,* p. Hg-101–Hg-300. Mineral. Soc. Am. Short Course Notes, Vol. 3.

Hanson, G. N. and R. Malhotra (1971) K–Ar ages of mafic dikes and evidence for low-grade metamorphism in northeastern Minnesota. *Geol. Soc. Am. Bull., 82,* 1107–1114.

Immega, I. P. and C. Klein, Jr. (1976) Mineralogy and petrology of some metamorphic Precambrian iron-formations in southwestern Montana. *Am. Mineral., 61,* 1117–1144.

Jaffe, H. W., P. Robinson and R. J. Tracy (1978) Orthoferrosilite and other iron-rich pyroxenes in microperthite gneiss of the Mount Marcy area, Adirondack Mountains. *Am. Mineral., 63,* 1116–1136.

Klein, C. (1966) Mineralogy and petrology of the metamorphosed Wabush Iron Formation, Southwestern Labrador. *J. Petrol., 7,* 246–305.

——— (1973) Changes in mineral assemblages with metamorphism of some banded Precambrian iron formations. *Econ. Geol., 68,* 1075–1088.

——— (1978) Regional metamorphism of Proterozoic iron-formation, Labrador Trough, Canada. *Am. Mineral., 63,* 898–912.

Matsui, Y., Y. Syono, S.-I. Akimoto and K. Kitayama (1968) Unit cell dimensions of some synthetic orthopyroxene group solid solutions. *Geochem. J., 2,* 61–70.

Nitsan, U. (1974) Stability field of olivine with respect to oxidation and reduction. *J. Geophys. Res., 79,* 706–711.

Nunes, P. D. and G. R. Tilton (1971) Uranium–lead ages of minerals from the Stillwater Igneous Complex and associated rocks, Montana. *Geol. Soc. Am. Bull., 82,* 2231–2250.

Page, N. J. (1977) Stillwater Complex, Montana: rock succession, metamorphism, and structure of the complex and adjacent rocks. *U.S. Geol. Surv. Prof. Pap. 999.*

——— and W. J. Nokleberg (1974) Geologic map of the Stillwater Complex, Montana. *U.S. Geol. Surv. Misc. Invest. Series Map I-797.*

Papike, J. J., K. L. Cameron and K. Baldwin (1974) Amphiboles and pyroxenes: characterization of other than quadrilateral components and estimates of ferric iron from microprobe data (abstr.). *Geol. Soc. Am. Abstracts with Programs, 6,* 1058–1054.

———, A. E. Bence, G. E. Brown, C. T. Prewitt and C. H. Wu (1971) Apollo 12 clinopyroxenes: exsolution and epitaxy. *Earth Planet. Sci. Lett., 10,* 307–315.

Podpora, C. and D. H. Lindsley (1979) Fe-rich pigeonites: minimum temperatures of stability in the Ca–Mg–Fe quadrilateral. *Trans. Am. Geophys. Union (EOS), 60,* 420–421.

Simmons, E. C., D. H. Lindsley and J. J. Papike (1974) Phase relations and crystallization sequence in a contact-metamorphosed rock from the Gunflint Iron Formation, Minnesota. *J. Petrol., 15,* 539–565.

Smith, D. (1971) Stability of the assemblage iron-rich orthopyroxene–olivine–quartz. *Am. J. Sci., 271,* 370–382.

Williams, R. J. (1972) Activity–composition relations in the fayalite–forsterite solid solution between 900° and 1300°C at low pressures. *Earth Planet. Sci. Lett., 15,* 296–300.

Manuscript received, November 19, 1979;
accepted for publication, June 10, 1980.